

*Negar Reiskarimian,
Aravind Nagulu,
Tolga Dinc, and
Harish Krishnaswamy*

Nonreciprocal Electronic Devices

©ISTOCKPHOTO.COM/SLAVEMOTION

One of the earliest references to reciprocity as an underlying symmetry within a system dates back to the 1828 work of Green in electrostatics, relating the interchanging electric potential and charge density [1]. Through the next several decades, some of the brightest mathematicians and physicists in history, including Helmholtz, Rayleigh, and Lorentz, made various observations related to reciprocity in different branches of physics such as optics, acoustics, elastodynamics, and electromagnetics and formulated a number of theorems to explain these observations [2], [3]. Even today, more than 100 years after Lorentz's proof of reciprocity in electromagnetics, his theory is still widely in use.

Onsager won the 1968 Nobel Prize in chemistry solely for his contributions to thermodynamics published in a two-part paper titled "Reciprocal Relations in Irreversible Processes" [4], [5]. The reciprocal relations

were fairly well known in different branches of physics by the early 20th century; however, it took a while for these theories to be applied to electronic network theory. Some early efforts include the generalization of Rayleigh's theory and the proof of reciprocity in radiating and receiving antennas (ANTs) [6], [7] and Casimir's simplified derivation of reciprocal relations for electricity conduction based on Onsager's work [8]. Others also looked into circuit synthesis, applications, and solving inverse problems by taking advantage of reciprocity in network theory [7], [9], [10].

The reciprocity relations also spurred research into techniques that violate it. As early as 1885 [11], Rayleigh proposed an optical device "in which the otherwise general optical law of reciprocity shall be violated." In classical network theory, the symmetry of matrices (e.g., the admittance and impedance matrices) was usually taken for granted. That all changed in 1948, when Tellegen [12] hypothesized an electric nonreciprocal

Negar Reiskarimian (nr2475@columbia.edu), Aravind Nagulu (an2750@columbia.edu), and Harish Krishnaswamy (harish@ee.columbia.edu) are with Columbia University, New York, United States. Tolga Dinc (t-dinc@ti.com) is with Texas Instruments, Dallas, United States.

Digital Object Identifier 10.1109/MMM.2019.2891380

Date of publication: 7 March 2019

component, called a *gyrator*, as the fifth elemental circuit building block to accompany the resistor, the capacitor, the inductor, and the transformer. The addition of the gyrator enables the synthesis of any arbitrary nonreciprocal network. As Tellegen notes in his seminal paper, “The gyrator can be realized [...] by means of a gyromagnetic effect of a ferromagnetic medium.” His proposed gyrator can be described in terms of its *S*-parameters, as in (1). As can be seen, the ideal gyrator is perfectly matched at its two terminals, has zero loss, and exhibits an additional 180° phase shift in its transmission in one direction:

$$S_{\text{gyrator}} = \begin{bmatrix} 0 & -1 \\ 1 & 0 \end{bmatrix}. \quad (1)$$

Soon after Tellegen’s proposal, Hogan demonstrated the first linear time-invariant (LTI) microwave gyrator prototype based on Faraday rotation (see the “Violation Of Reciprocal Relations” section) in ferrite materials, as shown in Figure 1 [13]. Here, the plane of polarization for the propagating waves is represented by sine waves in either direction. From left to right, a net polarization rotation of 180° is imparted to the signal (90° because of the twist in the rectangular waveguide and 90° from the effect of Faraday rotation). In the reverse direction, the total rotation of the polarization plane is 0° (90° from the twist and -90° resulting from Faraday rotation), resulting in the nonreciprocal phase response expected from Tellegen’s gyrator.

A three-port circulator with unidirectional wave propagation between adjacent ports was implemented in [13], using the gyrator along with two hybrid couplers. Ideally, two-port isolators (with a unidirectional transmission) and three-port circulators have the following *S*-parameters:

$$S_{\text{Iso.}} = \begin{bmatrix} 0 & 0 \\ 1 & 0 \end{bmatrix}, S_{\text{Circ.}} = \begin{bmatrix} 0 & 0 & 1 \\ 1 & 0 & 0 \\ 0 & 1 & 0 \end{bmatrix}. \quad (2)$$

In the 1960s, while magnetic circulator technology was still

in its infancy, magnetic-free, temporally modulated nonreciprocal parametric devices gained considerable attention [14]–[16]. Traditional parametric amplifiers had no directionality; hence, for a practical design, they required nonreciprocal devices such as circulators to separate the input and output circuitry and improve the amplifier noise performance [17] [Figure 2(a)]. In [16], a unilateral amplifier design using a transmission line and two diodes was demonstrated [Figure 2(b)], in which the pump frequency (i.e., modulation frequency) is an odd multiple of the signal frequency, the transmission line is quarter-wavelength at the signal frequency, and the two varactors are driven with 90° phase-shifted modulation signals. Another interesting interpretation of the same concept was explored by Kamal in [14]; here, the author takes advantage

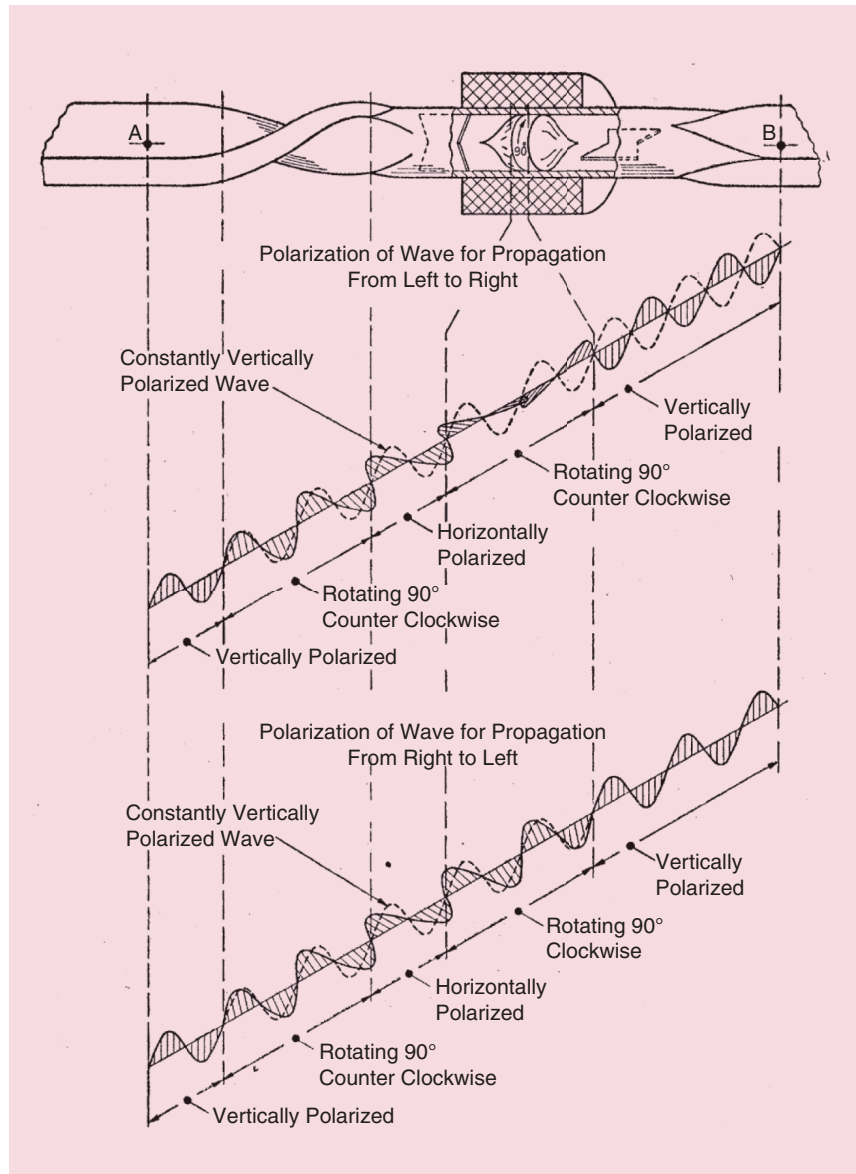


Figure 1. The microwave gyrator introduced by Hogan in [13] (top) and its operation principle as it appeared in the original manuscript (bottom).

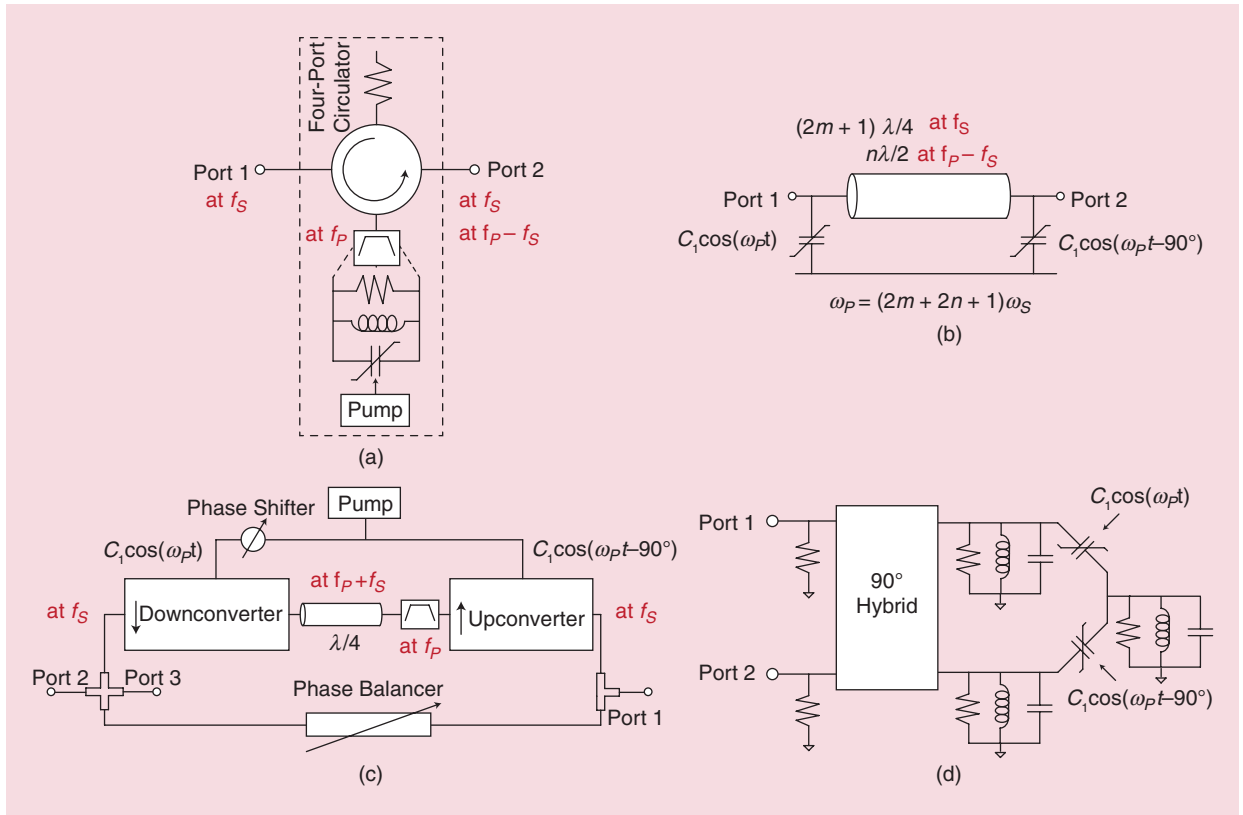


Figure 2. (a) A conceptual diagram of unilateral parametric amplification using a circulator to separate the input and output ports [17]. (b) The nonreciprocal parametric amplifier proposed in [16]. (c) A block diagram of the nonreciprocal parametric three-port circulator proposed in [14]. (d) A nonreciprocal parametric amplifier using a 90° hybrid [15].

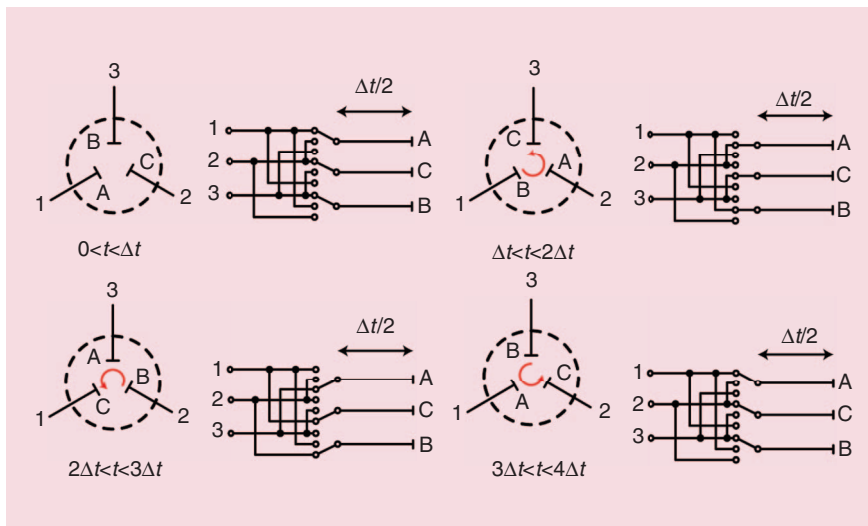


Figure 3. The linear, periodically time-varying RF circulator developed in [18] based on a switched-delay structure. A, B, and C are transmission lines terminated with short circuits for perfect reflection.

of the upconversion and downconversion characteristics of parametric amplifiers using phase-shifted modulation signals to create a gyrator and a three-port circulator [Figure 2(c)]. To implement the idea, he concludes that a

matching network is required between the two parametric devices, which turns out to be a quarter-wave transmission line, based on his analysis. Another unilateral amplifier architecture based on a 90° hybrid [Figure 2(d)] was proposed in [15].

Nonreciprocity has also been achieved by other forms of temporal modulation, such as switches controlled by a modulation signal at their gates. One of the first examples of such an approach can be found in a 1964 paper [18] in which a three-port circulator was demonstrated by taking advantage of a time-varying switched delay-line structure, as shown in Figure 3. In this figure, points A, B, and C are short terminations that provide perfect reflection of the incoming signal. A 100-MHz circulator was built (Figure 3), with a modulation frequency of 3.33 MHz and 33-ft delay lines.

Furthermore, active-biased, transistor-based architectures have been a popular alternative for achieving non-reciprocity, especially after the invention of the transistor and its widespread use in electronic circuits. In [19], an early example of such a device using three transistors in a loop was demonstrated across 30 Hz to 3 MHz (Figure 4).

Violation of Reciprocal Relations

The reciprocity theorem mandates an identical signal transmission profile for waves propagating in opposite directions between two points in space. Lorentz reciprocity describes the rules of reciprocity in the electromagnetic domain and is a fundamental physical precept that characterizes the vast majority of electronic and photonic materials, circuits, and components. Lorentz reciprocity (sometimes called the *Rayleigh–Carson reciprocity theorem*) can be described as

$$\iiint_V J_1 \cdot E_2 dV' = \iiint_V J_2 \cdot E_1 dV', \quad (3)$$

in which J_1 and J_2 are two arbitrary current source distributions and E_1 and E_2 are their respective electric fields induced in the space surrounding the sources. Equivalently, in circuit theory, this results in the symmetry of network matrices such as the impedance (Z), the admittance (Y), and the S -parameter matrix. Because of Lorentz reciprocity, any LTI system with symmetric permittivity and permeability tensors follows the rules of reciprocity.

Hence, to achieve nonreciprocal wave propagation, one of these necessary conditions must be violated: material systems with symmetric constituent tensors, linearity, or time invariance. Breaking the reciprocal relations enables new wave-propagation paradigms and the construction of nonreciprocal components and systems. Nonreciprocal devices, such as gyrators, isolators, circulators, unilateral parametric amplifiers, and nonreciprocal phase shifters, are essential for various applications at RF and millimeter-wave (mm-wave) frequencies, including communications, radar, sensing, imaging, and quantum signal processing.

Using the Faraday Effect

Historically, breaking reciprocity seemed to be possible only through the use of magnetic materials. Both Rayleigh’s proposal for nonreciprocal optical devices and Tellegen’s hypothesis for building a gyrator were based on the concept of Faraday rotation in ferromagnetic media through magneto-optic interactions or purely magnetic effects. Magnetic materials enable nonreciprocal wave propagation because they lose their symmetric permittivity or permeability tensors under the application of a magnetic field.

If an RF magnetic field of $\vec{H}_{RF} = \hat{x}H_x + \hat{y}H_y + \hat{z}H_z$ is applied to a large region of ferromagnetic material, which

Breaking the reciprocal relations enables new wave-propagation paradigms and the construction of nonreciprocal components and systems.

is under a constant magnetic bias of $\hat{z}H_0$ as shown in Figure 5(a), a magnetization field $\vec{M} = \hat{x}M_x + \hat{y}M_y + \hat{z}M_z$ is induced in the material in the form of [20] (4),

$$\vec{M} = [\chi]\vec{H}_{RF} \equiv \begin{bmatrix} M_x \\ M_y \\ M_z \end{bmatrix} = \begin{bmatrix} \chi_{xx} & \chi_{xy} & 0 \\ \chi_{yx} & \chi_{yy} & 0 \\ 0 & 0 & 0 \end{bmatrix} \times \begin{bmatrix} H_x \\ H_y \\ H_z \end{bmatrix}, \quad (4)$$

where χ_{ij} s are the magnetic susceptibilities. As a result, the magnetic flux density in an isotropic material can be defined as

$$\vec{B} = \mu_0(\vec{H}_{RF} + \vec{M}) = [\mu]\vec{H}_{RF} = \begin{bmatrix} \mu_1 & j\mu_2 & 0 \\ -j\mu_2 & \mu_1 & 0 \\ 0 & 0 & \mu_0 \end{bmatrix} \vec{H}_{RF}, \quad (5)$$

where μ_0 is the permeability of free space; $[\mu]$ is the permeability tensor, i.e., $\mu_1 = \mu_0(1 + \chi_{ii})$; $i = x, y$; and $\mu_2 = -j\mu_0\chi_{xy} = j\mu_0\chi_{yx}$.

Solving Maxwell’s equations for such an asymmetric permeability tensor results in different wave vectors for the left- and right-handed circular polarizations (β_{\pm}) and, hence, a rotation in the polarization vector of the electric field ($\theta_F(z)$) propagating through the media, as shown in Figure 5:

$$\theta_F(z) = -\left(\frac{\beta_+ - \beta_-}{2}z\right), \quad \beta_{\pm} = \omega\sqrt{\varepsilon(\mu_1 \pm \mu_2)}, \quad (6)$$

where ω and ε are the angular frequency of the wave and the permittivity of the medium, respectively. A distinct physical behavior also exists for optical frequencies because of magneto-optic interactions, resulting

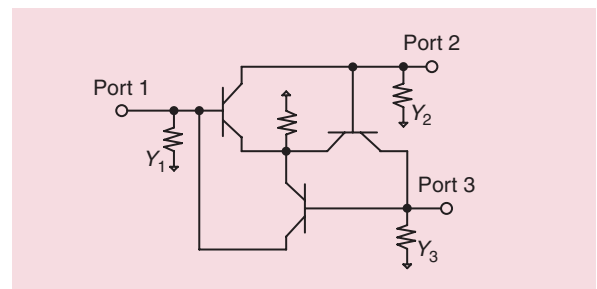


Figure 4. A three-port circulator based on active-biased transistors in a loop [19].

Ferrite materials are not compatible with integrated circuit technology because of the high-deposition temperatures required.

in an asymmetric permittivity tensor, which leads to a similar rotational effect [21].

Nonreciprocal components based on Faraday rotation in ferrite materials have been extensively investigated over the years by the microwave community. High-performance, high power-handling [third-order input intercept point (IIP3) exceeding +70 to +80 dBm at low-RF frequencies] ferrite circulators and isolators are commercially available from 10 s of MHz to more than 100 GHz [22].

The disadvantages of ferrite-based nonreciprocal devices are as follows.

- 1) The size of ferrite circulators based on waveguides or transmission lines is generally comparable to their operation wavelength. As a result, circulators at low RF frequencies can be extremely bulky.
- 2) In the mm-wave regime, the size of devices is smaller; however, the Faraday effect is weaker, and the magnetic materials become lossier. Similarly, the magneto-optic effect is usually weak and very lossy at optical frequencies [23].

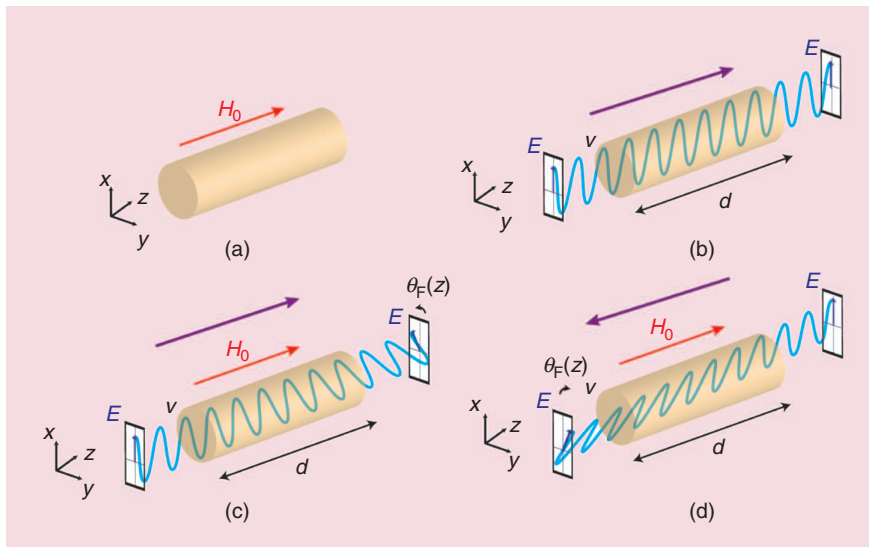


Figure 5. The concept of Faraday rotation. (a) A material of length d and an applied magnetic field of H_0 . (b) A wave propagating in the material experiences no Faraday rotation in the absence of the magnetic bias. (c) In the presence of a magnetic bias in the positive z direction, a wave traveling from left to right experiences Faraday rotation because of the difference in the propagation velocities of right-handed and left-handed circularly polarized waves, whereas (d) a wave traveling in the negative z direction experiences an opposite rotation.

- 3) Ferrite materials are not compatible with integrated circuit (IC) technology because of the high-deposition temperatures required [24]. As a result, ferrite nonreciprocal components cannot be integrated with the rest of the electronics to realize chip-scale, fully integrated systems.
- 4) Finally, ferrite circulators are also costly, and their cost does not readily scale through mass production, as is the case with IC technology. Readers are referred to [24] and [25] for a detailed bibliography of ferrite-based RF and microwave nonreciprocal devices.

Using Active-Biased Transistors

An alternative to using magnets is to exploit the inherent nonreciprocity of active current-/voltage-biased transistors. With the advent of transistors, active circulators became popular for low-frequency applications, where ferrite circulators did not exist (i.e., below 100 s of MHz), in applications with relatively low power handling, in cost- and size-limited implementations, and in scenarios where frequency tuning was of importance.

Active three-port nonreciprocal devices can be classified into two groups: circulators and quasi-circulators (QCs). QCs are three-port devices in which the transmission happens only between two pairs of ports: the third pair of ports is isolated in both directions (7). Fully symmetric active circulators can raise stability concerns and, hence, are usually realized with some loss [26]. QCs are of interest in transceivers, where transmitter (Tx)-to-

ANT and ANT-to-receiver (Rx) transmissions are necessary and the Tx and Rx are always isolated. They can also provide gain in the two transmission directions [26], [27]. Each of the circulator and QC categories can be implemented using only transistors and lumped components, as shown in [19] (Figure 4) or can combine active and distributed microwave components, such as hybrids and couplers [26]:

$$S_{QC} = \begin{bmatrix} 0 & 0 & 0 \\ 1 & 0 & 0 \\ 0 & 1 & 0 \end{bmatrix}. \quad (7)$$

Figure 6 shows an example block diagram and implementation for a fully integrated QC [27]. Here, port 1 is connected to a transistor-based, unilateral (nonreciprocal), in-phase (IP)/out-of-phase (OoP) divider,

one arm of which is connected to port 2, thus establishing transmission from port 1 to port 2. The other arm is combined with the signal from port 2 in a unilateral OoP/IP combiner to create destructive interference at port 3 (and, hence, isolation between ports 1 and 3). More recent examples of active circulators and QCs can be found in [28] and [29].

Another example of active devices used to enable nonreciprocity is demonstrated in [21] and [30]. These nonreciprocal components are built using transistor-loaded ring resonators that allow only a unilateral current to flow inside the loop and create a unidirectional rotating magnetic moment similar to the effect of Faraday rotation. The implementation of a nonreciprocal isolator and circulator using this idea is shown in Figure 7. While the basic operating principle is no different from the lumped active circulators described previously, the coupling of many such transistor-loaded ring resonators together can realize a nonreciprocal metamaterial or synthetic medium.

Active approaches are compatible with IC integration and have applications in low-power communication [29] and biomedical systems [31] but, eventually, are limited by the noise and nonlinearity introduced by the active devices [26]. As a result, they do not find utility at the front end of transceivers for traditional wireless communication and radar applications, where Tx power handling and Rx noise performance are paramount.

Using Nonlinearity

As discussed previously, another avenue for achieving nonreciprocity is by exploiting nonlinearity in a material or circuit. An example at optical frequencies is the Kerr effect,

in which the permittivity of the medium is nonlinear and electric-field dependent. In a third-order nonlinear material, ϵ can be described as

$$\epsilon \simeq \epsilon_0(\chi^{(1)} + 3\chi^{(3)}|E|^2), \quad (8)$$

where $\epsilon_0\chi^{(1)}$ is the linear permittivity of the medium, $\chi^{(3)}$ is the third-order nonlinear susceptibility, and E is the electric field intensity [32].

In such a nonlinear system, an asymmetric physical geometry can translate into an asymmetric wave propagation. For example, consider the following intuitive example taken from [33] (Figure 8). Here, we have a cascade of two media: one lossless and linear (ϵ_1) and one nonlinear with a complex permittivity of $\epsilon_2 - j\epsilon_2''(E)$ (i.e., higher loss for larger signals). Let us further assume that there is a strong mismatch between the two media, causing a significant reflection of signal energy at their interface. If a signal enters this combined structure from the left-hand side [Figure 8(a)], it travels through the linear medium without losing any energy. By the time it reaches the interface, most of the signal bounces back, and a small portion passes through to the nonlinear side. If the signal is small enough not to trigger the nonlinear behavior, it can go through the system without losing any further energy.

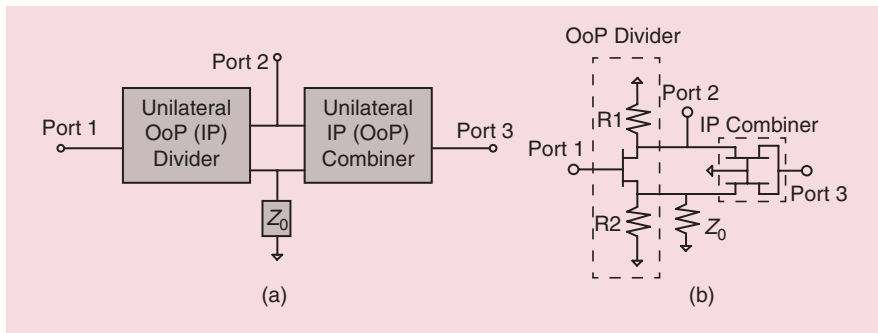


Figure 6. (a) A QC conceptual diagram. (b) The schematic of the MMIC QC implemented in [27].

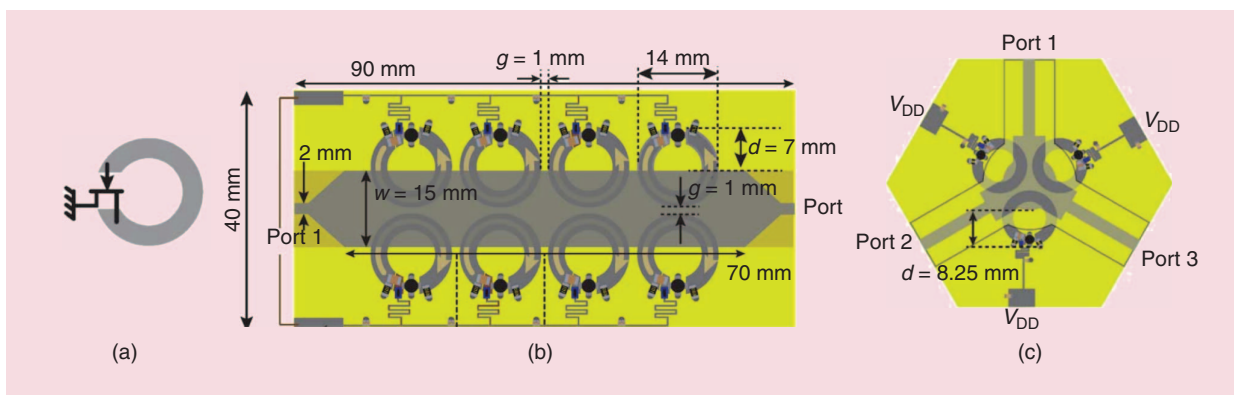


Figure 7. (a) The field-effect transistor loaded ring resonator concept. The (b) isolator and (c) circulator prototypes developed in [30].

In contrast to the low-permittivity modulation index of varactors, a transistor switch can provide an orders of magnitude higher conductivity modulation index.

However, in the reverse direction, the nonlinear medium attenuates the signal exponentially (because much higher power is present in the nonlinear medium, the imaginary part of the permittivity increases); hence, very little signal finds its way to the linear medium and the output.

An RF implementation of an isolator based on the third-order nonlinearity of resonators has been demonstrated using a cascade of a nonlinear Lorentzian resonator and a nonlinear Fano resonator [32], as shown in Figure 9. The nonlinear resonators are built by taking advantage of the nonlinear capacitance of variable capacitors (varactors).

Some of the disadvantages of the nonlinear approach include the following.

- 1) The extent of the nonreciprocal response is signal-power dependent and usually occurs for only a certain range of signal powers. As a result, it is not

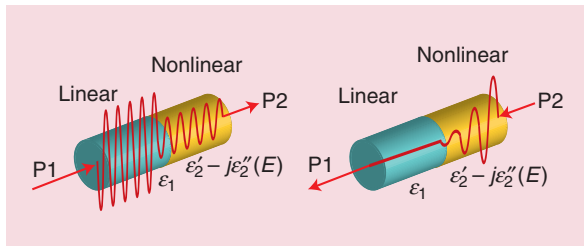


Figure 8. A principle of nonlinear nonreciprocity with an asymmetric physical geometry and a strong mismatch at the interface between the two media [33].

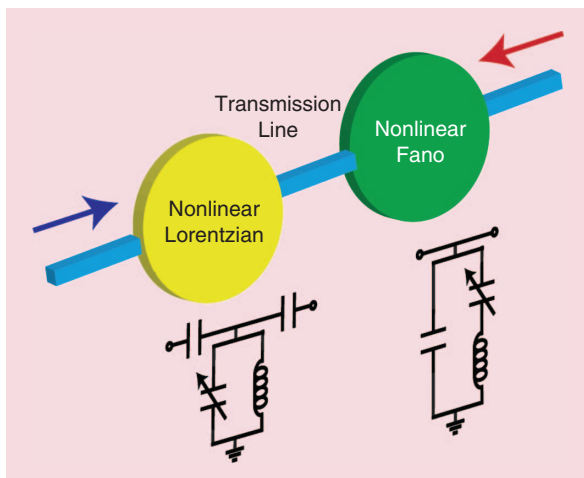


Figure 9. A block diagram of the nonlinear isolator implemented in [32].

suitable for applications where linearity is critical, such as wireless communications.

- 2) The nonreciprocity can be seen only if the device is excited one port at a time [34].

Using Time Variance

As mentioned previously, violating time invariance can also lead to nonreciprocity, the earliest examples of which include nonreciprocal parametric amplifiers [14]–[17], as shown in Figure 2. These nonreciprocal parametric amplifiers were based on two important concepts: 1) the availability of varactors that can be temporally modulated using a pump signal and 2) the introduction of a dynamic pump in time and space (note the two varactors in each example). Consider a nonlinear voltage-controlled varactor whose charge–voltage relationship is expressed by the following Taylor series:

$$q(t) = C_0 v(t) + a_2 v^2(t) + a_3 v^3(t) + \dots, \quad (9)$$

where C_0 is the static capacitance and a_i s are the higher-order nonlinear coefficients. Ignoring all of the higher-order terms except the first- and second-order terms, a modulation voltage of $v_m \cos(\omega_m t + \phi_m)$ across the capacitor results in a voltage-dependent variable capacitance of $C(v, t) = C_0 + a_2 v_m \cos(\omega_m t + \phi_m)$. For a single-tone input voltage at ω_{in} , it can be shown that the current passing through such a capacitor contains tones at ω_{in} as well as $\omega_m \pm \omega_{in}$. While the basic operating principle of a parametric amplifier has been studied with such a nonlinear device, the nonlinearity is not central to achieving a parametric response. Assuming that we can build a voltage-independent varactor where the modulation is caused by another force (e.g., a mechanical force changing the distance between the plates of a parallel-plate capacitor), similar frequency translation properties are attainable. Similar spatiotemporal modulation techniques have been explored in optics as well, examples of which can be found in [35] and [36].

More recently, there has been further progress made on breaking reciprocity in electronics through time variance, specifically spatiotemporal modulation of material parameters such as permittivity, permeability, and conductivity [23], [37]–[58]. Such approaches are theoretically noise-free and can be linear to the desired signal.

Many recent approaches have focused on permittivity as the modulated parameter [23], [37]–[40], [42], [43], [59]. In the RF domain, permittivity modulation is achieved using varactors that exhibit a limited modulation index (e.g., $C_{max}/C_{min} \sim 1.5$ in the implementation of [37]). In general, in both the microwave and optical domains, permittivity modulation is quite weak and associated with loss, particularly as the frequency increases. For instance, CMOS varactors are prohibitively lossy at mm-wave frequencies. Permeability modulation has also

been investigated, specifically using Josephson junctions as nonlinear inductors [44]–[47]. More recently, we have introduced conductivity modulation as an alternative approach to achieving nonreciprocity in time-varying systems. In contrast to the low-permittivity modulation index of varactors, a transistor switch can provide an orders of magnitude higher conductivity modulation index. A review of these recent approaches is provided in the sections that follow.

Parametric Modulation

A more recent example of a parametric design was demonstrated in [37], where the parametric modulation is performed along a quasi-distributed transmission line. The transmission line is loaded with varactors modulated by a traveling single-tone carrier such that $C(z, t) = C_0(1 + \xi_\epsilon \cos(\omega_m t - \beta_m z + \phi_m))$ (Figure 10), in which C_0 is the average capacitance, $\xi_\epsilon = C_m/C_0$ is the modulation index, C_m is the amplitude of the modulated capacitance, and β_m and ϕ_m are the wave vector and phase constant of the modulating carrier, respectively.

A simplified analysis of such a structure was carried out in [37], which shows that input signals launched in the same direction as the modulation carrier gradually convert to the frequency-shifted side-bands as z increases. At $z = \lambda_{in}/\xi_\epsilon \sqrt{2}$, where λ_{in} is the wavelength of the input signal, all of the signal power is converted to the mixing terms. The smaller the modulation index ξ_ϵ , the longer the length required for a full harmonic conversion, increasing the dimensions of the device. If the modulation frequency is higher than the signal frequency, the signal can also have a gain proportional to the frequency ratio of the upconverted and input signals.

For signals propagating in the opposite direction, it has been shown that no harmonic conversion takes place. A tradeoff exists between the choice of f_m , the power consumption in the modulation path, and the gain of the frequency-translated signal. Additionally,

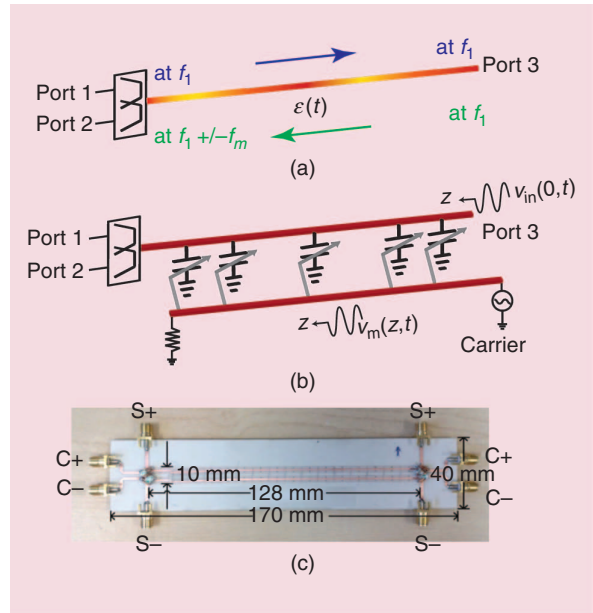


Figure 10. (a) The concept and (b) schematic of a parametric, time-varying transmission line and its frequency conversion. The printed circuit board (PCB) of the implementation in [37].

the noise performance of such approaches depends on the loaded quality factor of the transmission line, the quality factor of the individual varactors, and the permittivity modulation index [37]. Although not discussed in [37], phase noise in the modulation signal can also impact noise performance. Finally, the effect of noise folding from the sidebands should be taken into account and can be minimized by a low-pass filter at the input.

Angular Momentum Biasing

Inspired by Faraday rotation, a nonreciprocal response can also be achieved using angular-momentum biasing of a resonant ring [38]. An effective electronic spin is enabled by the spatiotemporal permittivity modulation

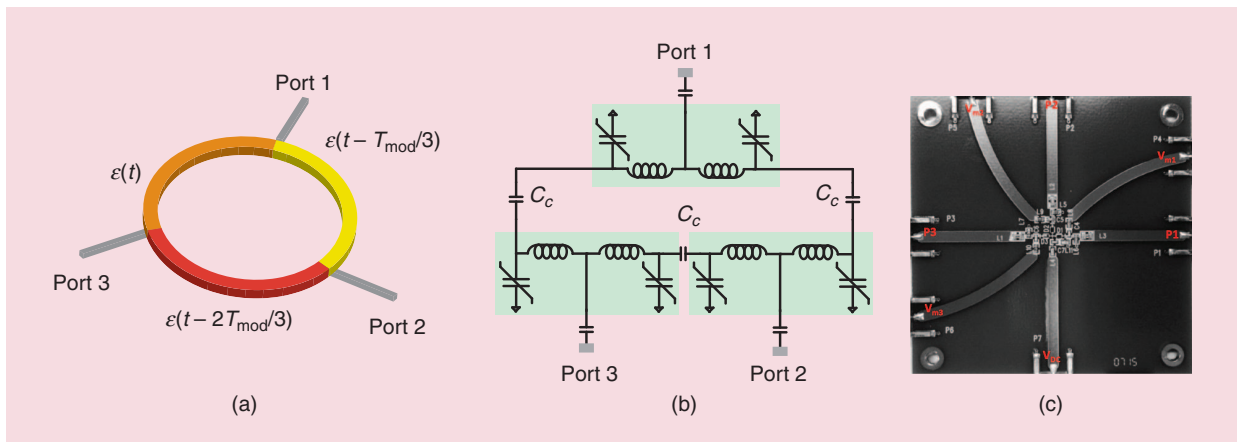


Figure 11. (a) Spatiotemporal permittivity modulation in a ring resonator, (b) the implementation of a ring resonator by three separate LC tanks, and (c) the PCB of the implementation in [60].

N-path filters have reemerged, primarily because of the availability of high-speed switches in integrated CMOS technology to realize tunable RF high Q filters.

with a traveling wave along the ring (Figure 11). Additionally, resonators can be used to miniaturize the size of the ring significantly, while boosting the weak permittivity modulation effect because of the limited modulation ratio, resulting in a stronger nonreciprocal response at the subwavelength scale. The resonators (bandpass or bandstop) can be connected together in various forms, such as delta or wye topologies [39], [60]. The resonators must exhibit high loaded Q to achieve significant impedance change, and this limits the operation's bandwidth. Additionally, the inductors and the varactors must have even higher unloaded Q to achieve low loss, which is fundamentally challenging, particularly on integrated semiconductor substrates.

It is shown in [61] that the bandwidth of the any pseudo-LTL, magnetic-free circulator is smaller than that of twice the modulating bandwidth. This implies that, for larger bandwidths, a higher modulation frequency is required. However, by increasing f_m , the dynamic power consumption is increased. Additionally, varactors—and permittivity modulation in general—also exhibit a tradeoff between modulation index and loss, particularly as the operating frequency is increased. Similar to parametric approaches, the noise performance in angular-momentum-based devices depends on the resonators' loaded Q and the unloaded Q of the varactors. Phase noise in the modulation signal can also impact the noise figure by creating random variation in the harmonic S -parameters. Proper design of the modulation circuitry can lower such undesired effects, and a noise figure close to the insertion loss can be achieved [39].

Conductance Modulation

In the circuits community, temporally modulated systems are commonly known as *linear periodically time-varying (LPTV)* circuits. One of the earliest reports on LPTV circuits dates back to 1947 [62], as shown in Figure 12. Here, a rotating brush periodically contacts a bank of capacitors to essentially commutate the signal across the capacitors, realizing a comb filter at harmonics of the rotation frequency. Such commutated networks came to be called *N-path filters*. In subsequent decades, commutated networks attracted considerable attention [63]–[65].

More recently, N-path filters have reemerged, primarily because of the availability of high-speed switches in integrated CMOS technology to realize tunable RF high Q filters [66], [67]. A transistor switch can have an orders of magnitude higher modulation index ($\xi_R = R_{OFF}/R_{ON}$ in the order of $10^3 - 10^5$) than the permittivity modulation index of a varactor (ξ_ϵ). Recently, we have shown for the first time that integrated LPTV circuits enable nonreciprocity through the spatiotemporal modulation of the conductivity of a medium [48]–[58], [68].

The following sections review our recent results on commutated network-based CMOS circulators spanning RF to mm-wave frequencies.

N-Path Filter-Based Nonreciprocal Devices

It has been shown that applying a relative phase shift to the nonoverlapping clocks driving the input and output switch sets of a two-port N-path filter imparts a nonreciprocal phase shift to the signals traveling in the forward and reverse directions because they see a different ordering of the phase-shifted switches [68] [Figure 13(a)]. Essentially, the two-port N-path filter with a clock phase shift of 90° realizes an electrically infinitesimal gyrator without the need for bulky passives such as inductors or transmission lines.

To convert phase nonreciprocity to nonreciprocal wave propagation, an N-path filter with $\pm 90^\circ$ phase shift is placed inside a transmission line loop having a length

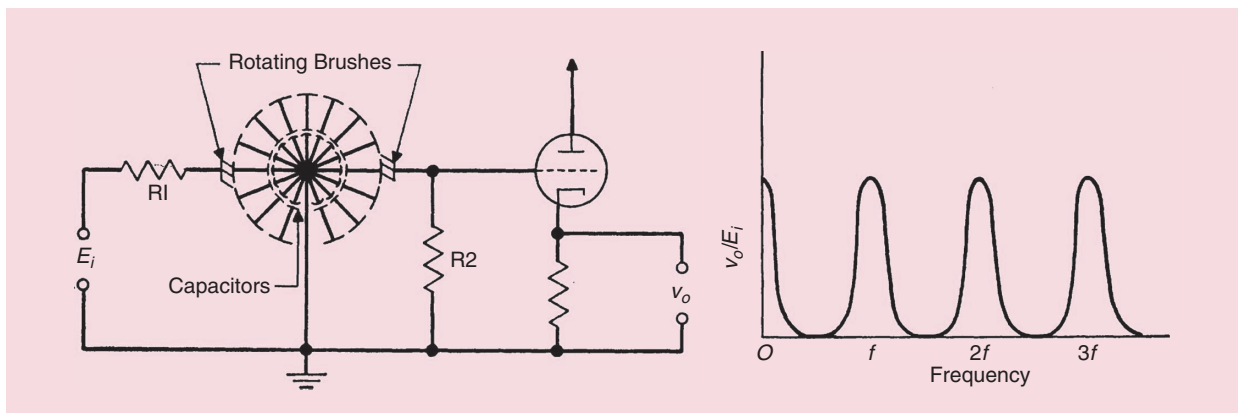


Figure 12. An early mechanical implementation of commutated networks [62].

of $3\lambda/4$ [50]. The combination of the N-path filter's nonreciprocal phase shift with the transmission line's reciprocal phase shift results in unidirectional wave propagation. Additionally, a three-port circulator can be realized by placing ports anywhere along the loop, as long as a $\lambda/4$ circumferential distance is maintained

between them. Maximum linearity with respect to the Tx port is achieved if the circulator is designed asymmetrically and the Rx port is placed adjacent to the N-path filter, because the inherent Tx–Rx isolation suppresses the voltage swing on either side of the N-path filter, thus enhancing its linearity to Tx signals [Figure 13(b)].

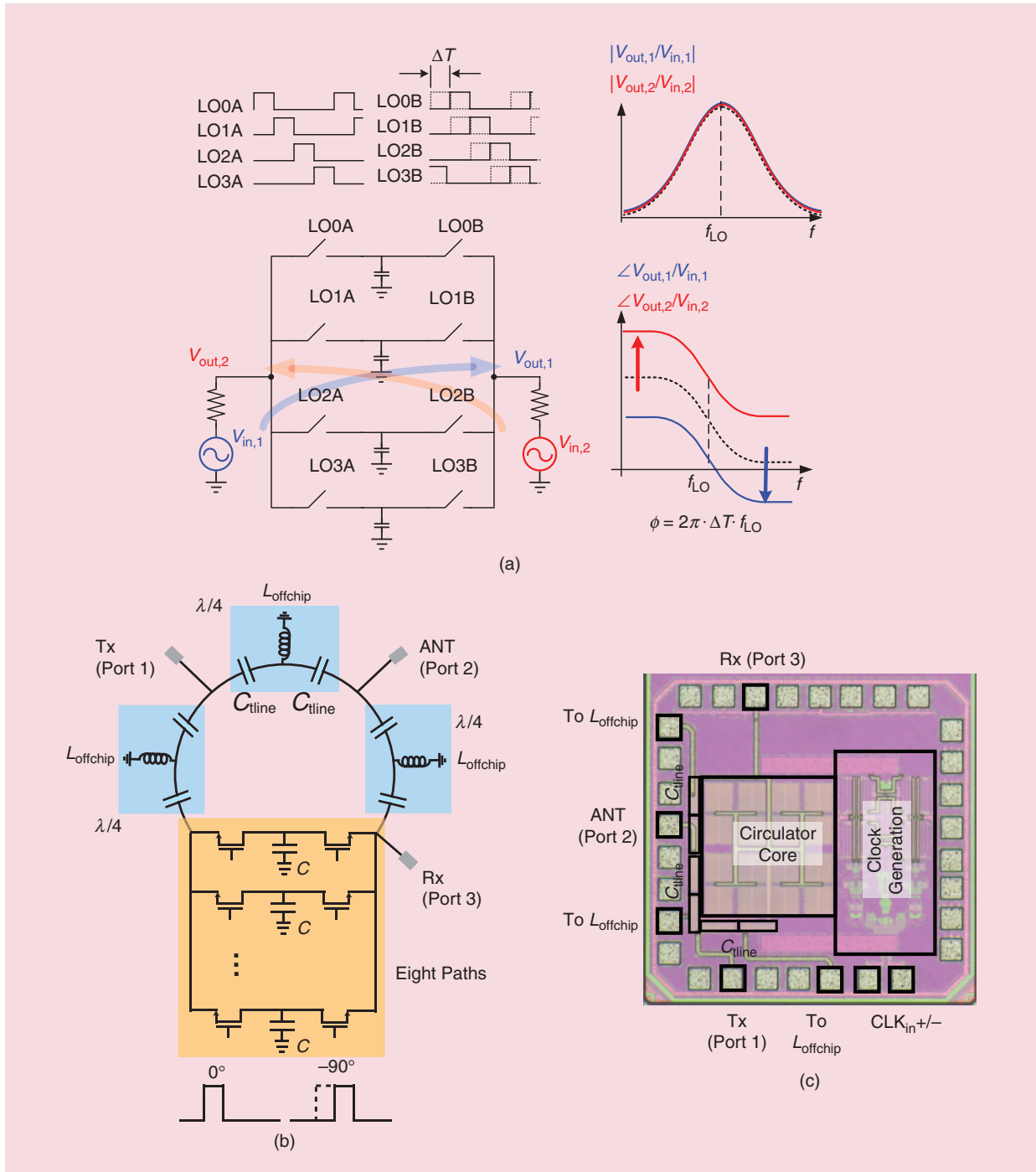


Figure 13. (a) The phase nonreciprocity of an N-path filter. (b) A schematic and (c) chip photo of a 65-nm RF magnetic-free passive N-path filter-based circulator employing a linearity-enhancement technique for Tx-side excitations [48], [50]. LO: local oscillator; CLK: clock.

Switched Transmission-Line-Based Nonreciprocal Devices

Inspired by the N-path filter-based RF circulator discussed previously, a generalized conductivity modulation concept is proposed using switched transmission lines [53], [55]. This structure consists of two sets of differential mixer-quad switches on either side of a differential transmission-line delay (replacing the commutated capacitors), as shown in Figure 14(a). The switches are clocked at a modulation frequency f_m , and the delay of the line is equal to $T_m/4$ ($1/4 f_m$). The switches are clocked using 50% duty-cycle square-wave clocks with a relative phase shift of $T_m/4$. As a result, waves traveling from left to right experience the transmission-line delay with no sign flips in either half of the clock period. On the other hand, waves traveling from right to left experience the transmission-line delay along with one sign flip.

In this structure, transmission in both directions is perfectly lossless, and there is an infinitely broadband 180° nonreciprocal phase difference. In other words, the structure realizes an infinitely broadband gyrator. The

key aspect of this architecture is that the infinite bandwidth of the gyrator implies that the signal frequency and modulation frequency are completely decoupled. An arbitrarily low-modulation frequency can be used, with the only restriction being an associated increase in the transmission line length, and hence, loss. This advantage has been leveraged to implement circulators at mm-waves while the modulation frequency is still at RF [54] and to implement RF circulators with high power handling through the use of high-voltage switches [56].

Another important feature of this infinitely broadband gyrator is that, while it is internally time-varying, it appears externally LTI, with no mixing products between the signal and the modulation seen at the ports. As a result, there is no folding of noise from other frequencies to the signal frequency of interest.

Similar ideas related to switched transmission lines used in realizing broadband nonreciprocity have been explored in [69], [70], and [71] (Figure 15). Recently, we have also shown that broadband transmission-line delay

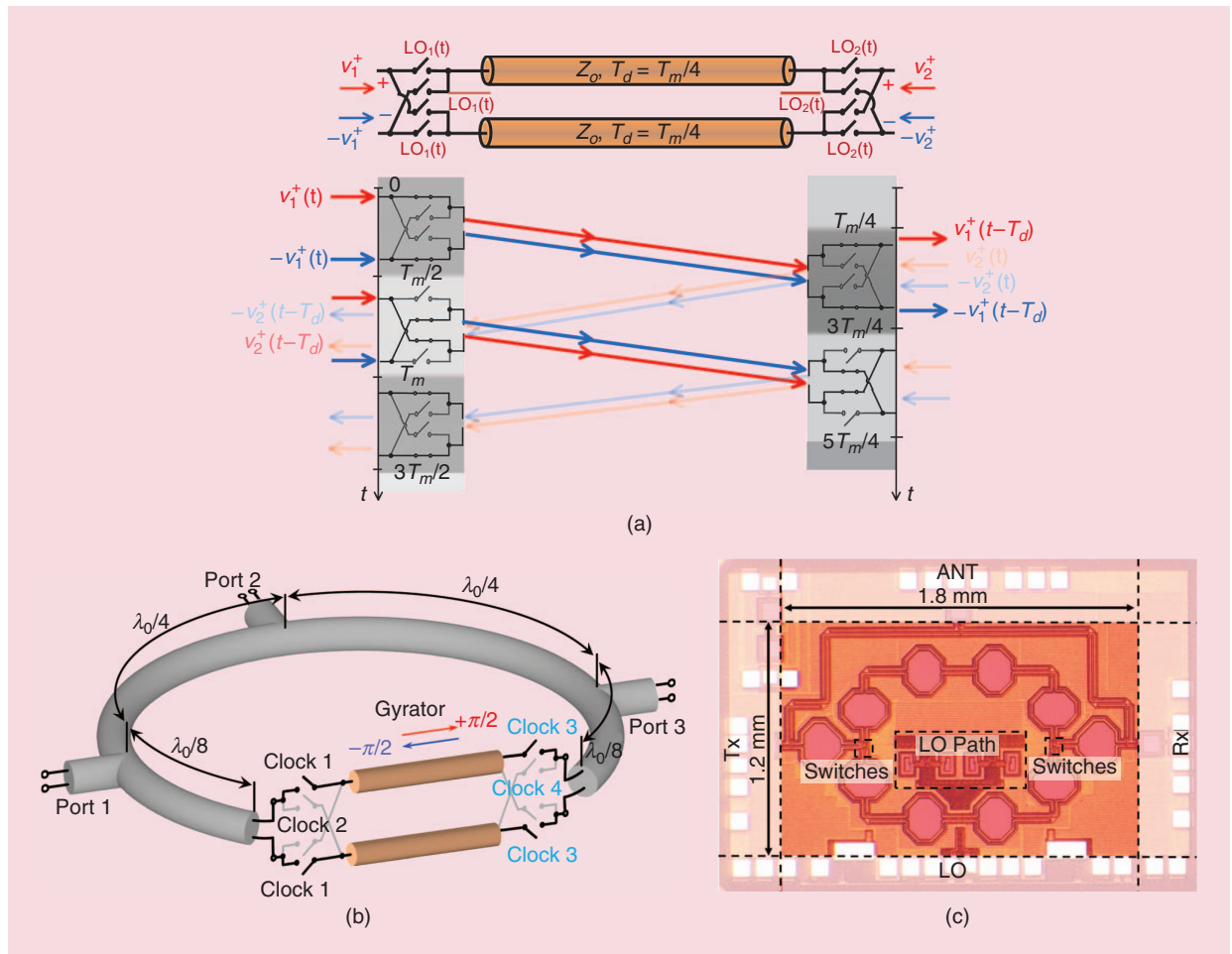


Figure 14. (a) A switched-transmission-line concept, (b) an mm-wave circulator based on switch-delay structure, and (c) a chip photo of the implemented 45-nm SOI CMOS 25-GHz mm-wave circulator [53]–[55].

can also be replaced with a bandpass delay structure, which offers certain design benefits that enable scaling to higher operating frequency at the expense of finite operating bandwidth [72].

Implementation Examples and State-of-the-Art Spatiotemporal Nonreciprocal Devices

Approaches Based on Permittivity Modulation

In [37], a nonreciprocal circulator is built using a parametric transmission line with distributed modulated capacitors, the concept for which was previously discussed. Because of the parametric nature of this device, the signals traveling in the same direction as the pump signal shift in frequency, while the signals traveling in the opposite direction pass through the device with no frequency shift; hence, an additional diplexer is required on one side to separate the incoming and outgoing waves, as shown in Figure 10. Moreover, to bring the signal back to its original frequency, additional frequency converters are required. Such a parametric structure can provide gain in the frequency-shifted path; however, there is a direct tradeoff between the power consumption of the clock generation circuitry and the maximum gain.

Various PCB based designs exploiting surface-mount components and using the angular momentum biasing technique have been reported in the recent past in the RF domain [39], [40], [61]; these have significant improvements over the original structure reported in [38]. Losses below 2 dB have been observed in a differential structure. Tx-ANT P1dBs approaching 1 W have been achieved as well. However, the IIP3 in the Tx-ANT path is limited to $\sim +30$ -dBm levels, rendering these prototypes unsuitable for commercial Wi-Fi or cellular applications where IIP3s of +50 to +70 dBm

are required. These prototypes may be useful in applications where the Tx signal is not modulated, such as RFID. Furthermore, a tradeoff exists between the maximum achievable isolation bandwidth and the device loss, because higher Q is required to lower the loss, in turn narrowing the bandwidth. Higher-order resonators or filters can be used to improve Q but at the cost of increased loss. Angular momentum biasing can also be implemented at mm-wave frequencies, an example of which is demonstrated in [73] using three parametric mixers in a loop. However, the poor Q of varactors at mm-waves results in high loss levels.

Moreover, the spatiotemporal modulation of permittivity can also be applied to the coupling between waveguides and resonators and so synthesize arbitrary nonreciprocal transfer functions [43], [74]. Table 1 provides a summary of state-of-the-art nonreciprocal circulators based on spatiotemporal modulation of permittivity.

Approaches Based on Conductivity Modulation

The first integrated, magnetic-free, conductivity-based passive circulator was demonstrated in a 65-nm CMOS technology in [48]–[50] (Figure 13). The circulator is implemented using a phase-shifted N-path filter surrounded by a $3\lambda/4$ transmission-line loop. It has been designed for an operation frequency of 750 MHz ($(f_{in}/f_m) = 1$) and achieves sub-2-dB loss between its Tx-ANT and ANT-Rx ports. It also takes advantage of the linearity enhancement technique for Tx-side excitations as described previously, improving the Tx-ANT IIP3 by roughly two orders of magnitude based on the measured performance.

The switched delay-line concept was exploited to realize a 25-GHz, fully integrated passive circulator in a 45-nm silicon-on-insulator (SOI) CMOS, as shown

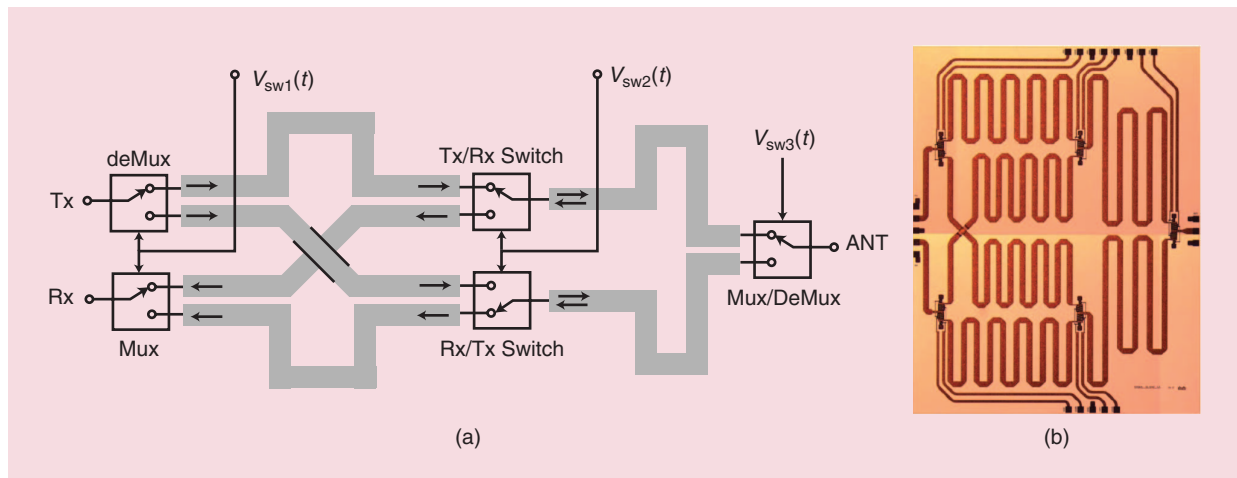


Figure 15. (a) The switched delay-line concept introduced in [69] and [70] and (b) a chip photo of a three-port circulator fabricated using the 0.2- μm GaN HEMT process. MUX: multiplexer.

TABLE 1. A performance summary of state-of-the-art nonreciprocal circulators based on spatiotemporal modulation of permittivity.

Reference	Technique	Frequency of Operation (GHz)	f_{in}/f_m	Tx-ANT/ ANT-Rx Transmission	Tx-Rx Isolation Bandwidth (BW)	Tx-ANT P1dB / IIP3	Platform
[37]	Parametric modulation	0.45–1.8	$\sim 0.11 - 0.43^1$	$\sim +0.35$ to $-1.5^{2,3}$ $\sim +1$ to -3.6 dB ^{2,3}	100% (>13 dB)	N/A / 33 dBm ⁴	PCB
[39]	Angular momentum	1	5.26	-3.3 to -3.56 dB ⁵	2.4% (>20 dB)	+29 / +33.7 dBm	PCB
[40]	Angular momentum	1	10	-1.78 to -2 dB ⁵	2.3% (>20 dB)	+28 / +31 dBm	PCB
[61]	Angular momentum	1	9.1	-4.2 to -5.8 dB / -4.25 to -5.5 dB ⁵	13.9% (>20 dB)	N/A	PCB
[73]	Angular momentum	85–110	7 ⁶	-4.8 to -5.8 dB ⁷	13.5% (>20 dB) ⁷	+11.2 dBm ³ / N/A	65-nm CMOS

¹ $f_m = 4.23$ GHz. ²Across the operation frequency range. ³Deduced from Figures 11 and 12 of [37]. ⁴Simulation result. ⁵At center frequency across the 20-dB isolation BW. ⁶At 100 GHz. ⁷Deduced from Figure 17(a) in [73].

in Figure 14 [53], [55]. Modulation was performed at one-third of the operating frequency (i.e., 8.33 GHz). The lowering of the modulation frequency, as well as the need for 50% duty-cycle clocks (as opposed to the numerous low duty-cycle clocks in N-path filters), is critical because clocking switches at mm-wave frequencies is impractical in current CMOS IC technology. The infinitely broadband phase nonreciprocity of the gyrator also implies a broader bandwidth of operation for the resultant circulator. This idea has also been extended to an implementation at 60 GHz with a f_{in}/f_m of 7 based on switching of bandpass delay lines, as discussed previously [72]. The impact of clock and transmission-line imperfections is discussed in further detail in [55],

which shows minimal penalty because of mismatched delay between the switches and the transmission line. Additionally, by reducing the modulation frequency, the effect of finite rise-and-fall times is minimized.

A more recent, highly linear RF circulator based on the switched-transmission line structure was reported in [56], demonstrating enhanced power handling and linearity at 1 GHz of operating frequency. The switches are modulated at 333 MHz, which enables the use of thick-oxide devices in 180-nm SOI CMOS technology to boost power handling to close to ~ 1 W (Figure 16). The Tx-ANT IIP3 exceeds +50 dBm, enabling this technique to approach the performance required for commercial Wi-Fi and cellular applications. Ongoing unpublished

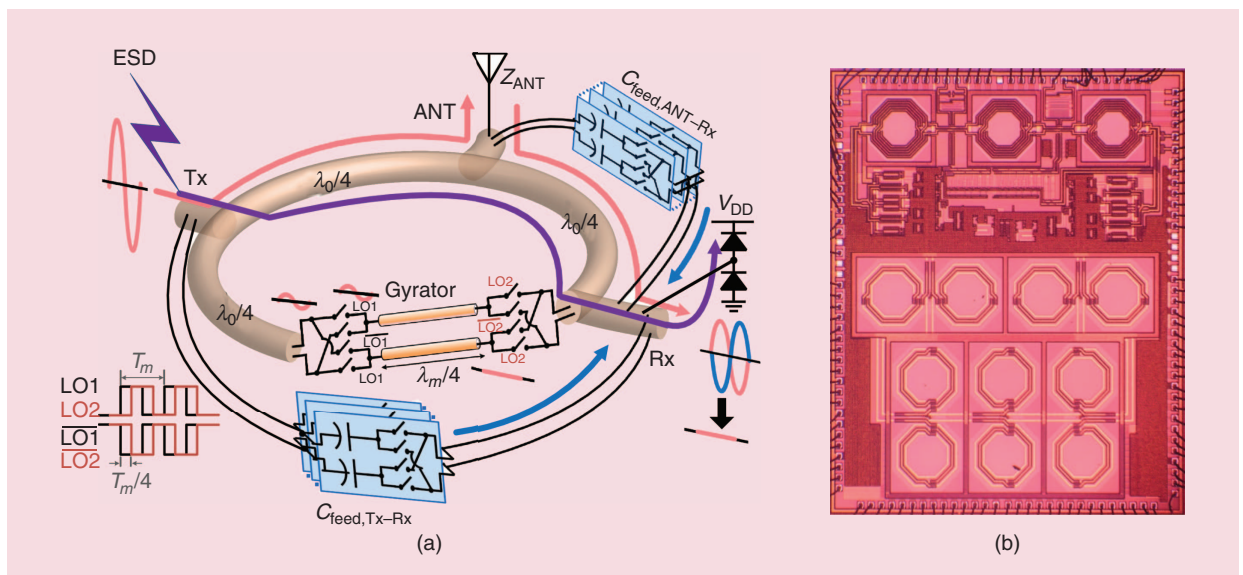


Figure 16. (a) An RF switched transmission-line circulator with >1-W power-handling capability and inductor-free ANT balancing. (b) A chip photo of a 180-nm SOI CMOS prototype implemented in [56]. ESD: electrostatic discharge.

research indicates the ability to boost power handling by another order of magnitude while maintaining/improving other performance metrics.

Additionally, we employ an ANT-balancing technique by using feed capacitors between the Tx–Rx and ANT–Rx ports to overcome the effect of limited isolation due to mismatches at the ANT port. Because there is a -90° inherent phase difference between the signals at the Tx and ANT ports and thanks to a differential implementation, orthogonal currents can be generated at the Rx port; hence, a complete coverage of a voltage standing-wave ratio of up to 1.85 can be achieved without any inductive or resistive elements. A summary of state-of-the-art nonreciprocal circulators based on the spatiotemporal modulation of conductivity is presented in Table 2.

The noise generated in conductivity-modulation-based approaches comes from three main sources: 1) the switch resistance of the transistors and limited Q of the transmission lines, 2) the noise folding from the harmonics, and 3) the effect of the phase noise of the modulating clock [39]. It has been shown that the noise figure of conductivity-modulation-based approaches can be as low as their insertion loss and, hence, mostly limited to the effect of switch resistance and the limited Q of the passives [55], [56]. Additionally, the performance of the nonreciprocal devices should be maintained, even under the application of a large-signal Tx or interferers. Further analysis of the interaction of modulation phase noise with the powerful Tx signal (reciprocal mixing-like effects) is an ongoing effort. More in-depth discussions of such effects can be found in [52] and [55].

RF Electroacoustics and Electromechanical Devices

To further increase the modulation frequency ratio (f_{in}/f_m) and lower the modulation path power consumption at the

expense of operating bandwidth, recent work has focused on using electroacoustic components such as surface acoustic wave (SAW) devices, film bulk acoustic resonators (FBARs), and other microelectromechanical (MEM) resonators, which provide much higher Q resonators and larger group delays compared to on-chip and surface-mount device passives.

In [76], a 1.95-GHz circulator was designed and implemented based on the conductivity modulation technique, with a SAW filter used as the delay medium between two sets of quad switches. The modulation frequency is chosen to be 50 MHz, and the measurements have shown close to a 3-dB loss and more than 40-dB isolation between the Tx and Rx ports (Figure 17).

The authors of [77] demonstrated an FBAR circulator based on the concept of angular momentum biasing. FBARs work at higher frequencies compared to SAW resonators. The 2.5-GHz prototype was built using three FBARs along with series varactors to modulate each resonator at a much lower frequency. The device achieves a very high f_{in}/f_m ratio but is extremely lossy (an 11-dB insertion loss). Another example using MEM resonators was shown in [78], where FBAR-based MEM tank circuits were exploited to design an angular momentum-biased circulator at 2.5 GHz with 4.2 dB of loss and high linearity (Figure 18). Other examples of these techniques have been demonstrated in [75], [79], and [80]. Table 3 provides a performance summary of recent work in the area. While these approaches provide much higher modulation frequency ratios, their performances are still far from the performances of the integrated approaches discussed previously.

Applications of Nonreciprocal Devices

Nonreciprocal components such as gyrators, isolators, circulators, unilateral parametric amplifiers, and nonreciprocal

TABLE 2. A performance summary of state-of-the-art nonreciprocal circulators based on spatiotemporal modulation of conductivity.

Reference	Technique	Frequency of Operation	f_{in}/f_m	Tx–ANT/ ANT–Rx Transmission	Tx–Rx Isolation BW	Tx–ANT P1dB /IIP3	P_{DC}	Platform
[50]	Conductivity modulation	610–975 MHz	1	–1.7/–1.7 dB	1.9% (>25 dB) 0.33% (>40 dB)	N/A / +27.5 dBm	59 mW	65-nm CMOS
[56]	Conductivity modulation	860–1,080 MHz	3	–2.1/–2.9 dB	17% (>25 dB) 3.1% (>40 dB)	+30.7 / +50 dBm	170 mW	180-nm SOI CMOS
[55]	Conductivity modulation	25 GHz	3	–3.3/–3.2 dB	18% (>18.5 dB)	+21.5 / +20.1 dBm	78.4 mW	45-nm SOI CMOS
[70]	Conductivity modulation	10 MHz–1.5 GHz	0.004 – 0.6 ¹	–5.4 to –7.5 dB	100% (>20 dB)	+9 dBm ² / N/A	560 mW	0.2- μ m GaN HEMT
[75]	Conductivity modulation	10–900 MHz	0.42 – 37.8 ³	–5.1 to –7.6 dB	100% (>24 dB)	N/A	N/A	PCB

¹ $f_m = 2.5$ GHz. ²At 200 MHz. ³ $f_m = 23.8$ MHz.
GaN: gallium nitride.

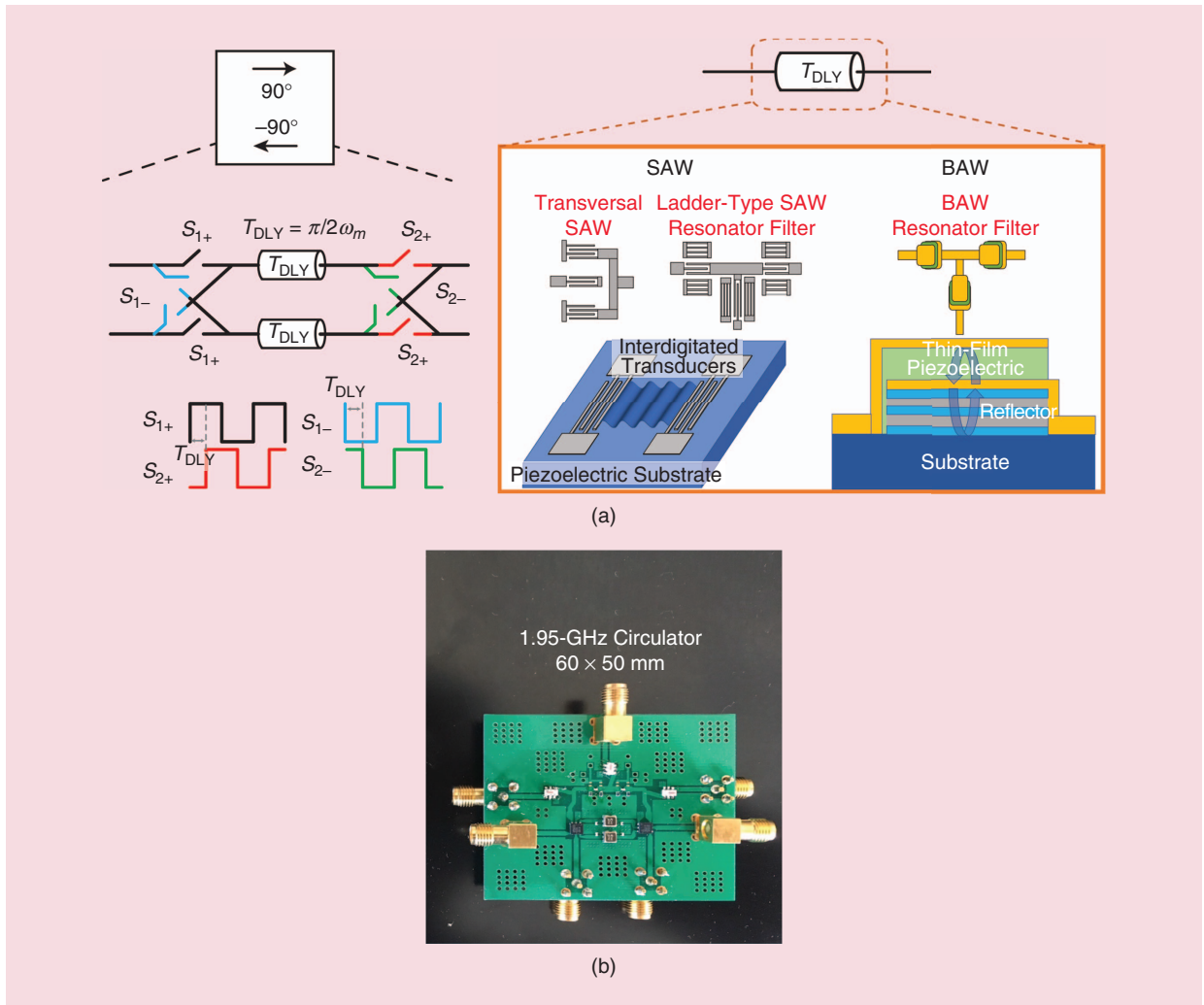


Figure 17. (a) A switched-filter gyrator using acoustic wave devices. (b) The PCB of the implemented 1.95-GHz three-port circulator using commercial SAW filters [76]. BAW: bulk acoustic wave.

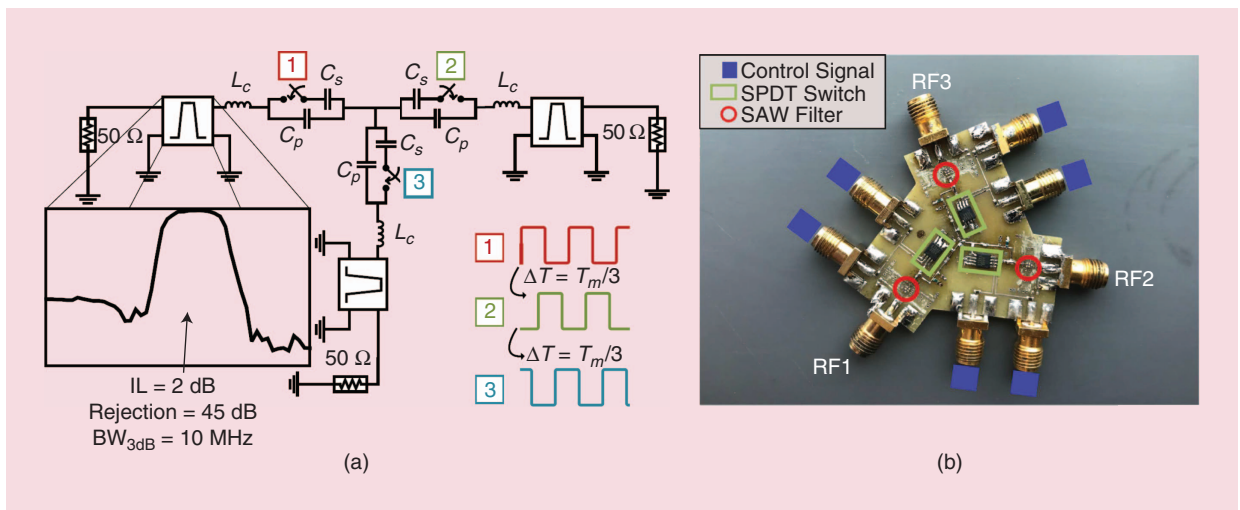


Figure 18. (a) A three-port angular momentum-based circulator using SAW filters and (b) its PCB implementation [79]. IL: insertion loss; SPDT single-pole double throw.

phase shifters are critical for various RF and mm-wave applications, including communications, radar, quantum signal processing, imaging, and sensing.

Circulators and isolators find applications in high-power cellular base stations and in U.S. Department of Defense radios to protect high-power amplifiers from back ANT reflections. High-performance circulators also find application as the shared ANT interface for transceivers in emerging wireless communication paradigms, such as full-duplex (FD) [81]–[84] and FD multiple-input, multiple-output systems [85], [86], and in frequency-modulated continuous-wave radar. FD aims to instantly double the link capacity in the physical layer, by simultaneously transmitting and receiving at the same frequency, and provide other benefits in the higher layers [83], [84]. Various implementations of FD systems with integrated N-path filter-based nonreciprocal ANT interfaces have been shown [51], [52], [86], [87], in which the N-path filter in the circulator can be repurposed as a downconverting mixer, directly providing the baseband received signals on the N-path filter capacitors [51]. N-path filter-based circulator Rx FD phased-array front ends can also enable baseband beamforming with minimal overhead, by virtue of their multiphase outputs [87]. Additionally, nonreciprocal ANT interfaces can incorporate the ANT tuner required for many wireless applications, an example of which (described previously) was implemented in [56].

Nonreciprocal components also find applications in solid-state superconducting quantum signal processing systems. Many quantum measurement setups have specific readout requirements, such as microwave reflection-based measurement setups using nonreciprocal devices to separate the input and output channels and also meet stringent noise requirements [44]–[47].

Nonreciprocal ANT interfaces can incorporate the ANT tuner required for many wireless applications.

Nonreciprocal devices have long been used in biomedical radar and imaging systems [31], [88]–[91]. To date, most such systems use either magnetic circulators or QCs. As the spatiotemporal modulation techniques to achieve nonreciprocity mature, it will be of interest to see how they can contribute to the next generation of biomedical systems and devices.

Conclusions

Thus far, nonreciprocal devices have been an integral part of many electrical and optical systems. Among the various approaches that enable nonreciprocity, the spatiotemporal modulation of material properties, e.g., permittivity and conductivity, has gained the most attention in the recent past because of its potential for noise-free, highly linear operation. These magnetic-free approaches are also compatible with IC technology, have much smaller form factors, and enable high performance and reconfigurable implementations. Tables 1–3 summarize the results of the most recent advances using spatiotemporal modulation.

Acknowledgments

This work was supported by the DARPA ACT and DARPA SPAR programs.

References

- [1] D. M. Cannell, *George Green: Mathematician and Physicist 1793–1841*, 2nd ed. Philadelphia, PA: Society for Industrial and Applied Mathematics, 2001, pp. 190–192.

TABLE 3. A performance summary of recent spatiotemporal electroacoustic nonreciprocal devices.

Reference	Technique	Frequency of Operation f_{in}	Modulation Frequency f_m	f_{in}/f_m	Tx–ANT/ANT–Rx Transmission (dB)	Tx–Rx Isolation (dB)	Tx–ANT P1dB/IIP3	Technology
[76]	Conductivity modulation	1.95 GHz	50 MHz	39	–3.63/–3.28	41.9	N/A/ +17.2 dBm	Quad switches plus SAW filters
[77]	Angular momentum	2.5 GHz	3 MHz	833.33	–11	76	N/A	FBAR die on PCB
[79]	Angular momentum	870 MHz	15 MHz	58	–8.5	>14	N/A	SAW filter plus SPDT GaAs SW also on PCB
[78]	Angular momentum	2.5 GHz	6 MHz	416.66	–4.2	18	+40 dBm / +28 dBm	FBAR-based MEM tanks
[80]	Angular momentum	145 MHz	120 kHz	1,208.33	–8	30	N/A	MEM resonators
[75]	Conductivity modulation	155 MHz	877.19 kHz	176.7	–6.6	25.4	>10 dBm / +30 dBm	Acoustic transducers

GaAs: gallium arsenide.

- [2] J. D. Achenbach, *Reciprocity in Elastodynamics*. Cambridge, U.K.: Cambridge Univ. Press, 2003.
- [3] R. J. Potton, "Reciprocity in optics," *Rep. Prog. Phys.*, vol. 67, no. 5, pp. 717–754, 2004.
- [4] The Nobel Prize, "Award ceremony speech," 2018. [Online]. Available: <https://www.nobelprize.org/prizes/chemistry/1968/ceremony-speech/>
- [5] L. Onsager, "Reciprocal relations in irreversible processes. I," *Phys. Rev.*, vol. 37, no. 4, pp. 405–426, 1931.
- [6] J. R. Carson, "Reciprocal theorems in radio communication," in *Proc. Inst. Radio Engineers*, vol. 17, no. 6, pp. 952–956, 1929.
- [7] S. Ballantine, "Reciprocity in electromagnetic, mechanical, acoustical, and interconnected systems," in *Proc. Inst. Radio Engineers*, vol. 17, no. 6, pp. 927–951, 1929.
- [8] H. B. G. Casimir, "On Onsager's principle of microscopic reversibility," *Rev. Mod. Phys.*, vol. 17, no. 2–3, pp. 343–350, 1945.
- [9] B. D. Tellegen, "A general network theorem, with applications," *Philips Res. Rep.*, vol. 7, pp. 256–269, 1952.
- [10] B. Bleaney and B. Bleaney, *Electricity and Magnetism*. London, U.K.: Oxford Univ. Press, 1965.
- [11] L. Rayleigh, "On the constant of magnetic rotation of light in bisulphide of carbon," *Philos. Trans. R. Soc. London*, vol. 176, pp. 343–366, 1885.
- [12] B. D. Tellegen, "The gyrator, a new electric network element," *Philips Res. Rep.*, vol. 3, no. 2, pp. 81–101, 1948.
- [13] C. L. Hogan, "The ferromagnetic Faraday effect at microwave frequencies and its applications: The microwave gyrator," *Bell Syst. Tech. J.*, vol. 31, no. 1, pp. 1–31, 1952.
- [14] A. Kamal, "A parametric device as a nonreciprocal element," in *Proc. IRE*, vol. 48, no. 8, pp. 1424–1430, 1960.
- [15] L. Baldwin, "Nonreciprocal parametric amplifier circuits," in *Proc. IRE*, vol. 49, no. 6, p. 1075, 1961.
- [16] J. Hamasaki, "A theory of a unilateral parametric amplifier using two diodes," *Bell Syst. Tech. J.*, vol. 43, no. 3, pp. 1123–1147, 1964.
- [17] E. D. Reed, "The variable-capacitance parametric amplifier," *IRE Trans. Electron. Devices*, vol. 6, no. 2, pp. 216–224, 1959.
- [18] R. J. Mohr, "A new nonreciprocal transmission line device," in *Proc. IEEE*, vol. 52, no. 5, p. 612, 1964.
- [19] S. Tanaka, N. Shimomura, and K. Ohtake, "Active circulators—the realization of circulators using transistors," in *Proc. IEEE*, vol. 53, no. 3, pp. 260–267, 1965.
- [20] D. M. Pozar, *Microwave Engineering*. Hoboken, NJ: Wiley, 2009.
- [21] T. Kodera and C. Caloz, "Unidirectional loop metamaterials (ULM) as magnetless artificial ferrimagnetic materials: Principles and applications. 2018. [Online]. Available: arXiv:1804.08719
- [22] JQL Electronics. Accessed on: 2018. [Online]. Available: <http://www.jqlelectronics.com/>
- [23] D. L. Sounas and A. Alù, "Non-reciprocal photonics based on time modulation," *Nature Photonics*, vol. 11, no. 12, pp. 774–783, 2017.
- [24] J. D. Adam, L. E. Davis, G. F. Dionne, E. F. Schloemann, and S. N. Stitzer, "Ferrite devices and materials," *IEEE Trans. Microw. Theory Techn.*, vol. 50, no. 3, pp. 721–737, 2002.
- [25] R. H. Knerr, "An annotated bibliography of microwave circulators and isolators: 1968–1975," *IEEE Trans. Microw. Theory Techn.*, vol. 23, no. 10, pp. 818–825, 1975.
- [26] G. Carchon and B. Nanwelaers, "Power and noise limitations of active circulators," *IEEE Trans. Microw. Theory Techn.*, vol. 48, pp. 316–319, Feb. 2000.
- [27] S. Hara, T. Tokumitsu, and M. Aikawa, "Novel unilateral circuits for MMIC circulators," *IEEE Trans. Microw. Theory Techn.*, vol. 38, no. 10, pp. 1399–1406, 1990.
- [28] T. Kijsanayotin and J. F. Buckwalter, "Millimeter-wave dual-band, bidirectional amplifier and active circulator in a CMOS SOI process," *IEEE Trans. Microw. Theory Techn.*, vol. 62, no. 12, pp. 3028–3040, 2014.
- [29] S. A. Ayati, D. Mandal, B. Bakkaloglu, and S. Kiaei, "Integrated quasi-circulator with RF leakage cancellation for full-duplex wireless transceivers," *IEEE Trans. Microw. Theory Techn.*, vol. 66, no. 3, pp. 1421–1430, 2018.
- [30] T. Kodera, D. L. Sounas, and C. Caloz, "Magnetless nonreciprocal metamaterial (MNM) technology: Application to microwave components," *IEEE Trans. Microw. Theory Techn.*, vol. 61, no. 3, pp. 1030–1042, 2013.
- [31] H.-C. Kuo et al., "A fully integrated 60-GHz CMOS direct-conversion Doppler radar RF sensor with clutter canceller for single-antenna noncontact human vital-signs detection," *IEEE Trans. Microw. Theory Techn.*, vol. 64, no. 4, pp. 1018–1028, 2016.
- [32] D. L. Sounas, J. Soric, and A. Alù, "Broadband passive isolators based on coupled nonlinear resonances," *Nature Electron.*, vol. 1, no. 2, p. 113, 2018.
- [33] C. Caloz, A. Alù, S. Tretyakov, D. Sounas, K. Achouri, and Z.-L. Deck-Léger, "Electromagnetic nonreciprocity," *Phys. Rev. Appl.*, vol. 10, no. 4, p. 047001, 2018.
- [34] Y. Shi, Z. Yu, and S. Fan, "Limitations of nonlinear optical isolators due to dynamic reciprocity," *Nature Photonics*, vol. 9, no. 6, pp. 388–392, 2015.
- [35] H. Lira, Z. Yu, S. Fan, and M. Lipson, "Electrically driven nonreciprocity induced by interband photonic transition on a silicon chip," *Phys. Rev. Lett.*, vol. 109, no. 3, p. 033901, 2012.
- [36] L. D. Tzuang, K. Fang, P. Nussenzweig, S. Fan, and M. Lipson, "Non-reciprocal phase shift induced by an effective magnetic flux for light," *Nature Photonics*, vol. 8, no. 9, pp. 701–705, 2014.
- [37] S. Qin, Q. Xu, and Y. Wang, "Nonreciprocal components with distributedly modulated capacitors," *IEEE Trans. Microw. Theory Techn.*, vol. 62, no. 10, pp. 2260–2272, 2014.
- [38] N. Estep, D. Sounas, J. Soric, and A. Alù, "Magnetic-free nonreciprocity based on parametrically modulated coupled-resonator loops," *Nature Physics*, vol. 10, no. 12, pp. 923–927, 2014.
- [39] A. Kord, D. L. Sounas, and A. Alù, "Magnet-less circulators based on spatiotemporal modulation of bandstop filters in a delta topology," *IEEE Trans. Microw. Theory Techn.*, vol. 66, no. 2, pp. 911–926, 2018.
- [40] A. Kord, D. L. Sounas, and A. Alù, "Pseudo-linear time-invariant magnetless circulators based on differential spatiotemporal modulation of resonant junctions," *IEEE Trans. Microw. Theory Techn.*, vol. 66, no. 6, pp. 2731–2745, 2018.
- [41] Y. Hadad, J. C. Soric, and A. Alù, "Breaking temporal symmetries for emission and absorption," in *Proc. Nat. Academy of Sciences*, 2016, p. 201517363.
- [42] S. Taravati, N. Chamanara, and C. Caloz, "Nonreciprocal electromagnetic scattering from a periodically space-time modulated slab and application to a quasi-sonic isolator," *Phys. Rev. B, Condens. Matter*, vol. 96, no. 16, p. 165144, 2017.
- [43] C. W. Peterson, S. Kim, J. T. Bernhard, and G. Bahl, "Reconfigurable arbitrary nonreciprocal transfer functions through nonreciprocal coupling. 2017. [Online]. Available: arXiv:1702.06476
- [44] A. Kamal, J. Clarke, and M. Devoret, "Noiseless non-reciprocity in a parametric active device," *Nature Physics*, vol. 7, no. 4, pp. 311–315, 2011.
- [45] J. Kerckhoff, K. Lalumière, B. J. Chapman, A. Blais, and K. W. Lehnert, "On-chip superconducting microwave circulator from synthetic rotation," *Phys. Rev. Appl.*, vol. 4, p. 034002, Sept. 2015.
- [46] B. J. Chapman et al., "Widely tunable on-chip microwave circulator for superconducting quantum circuits," *Phys. Rev. X*, vol. 7, no. 4, p. 041043, 2017.
- [47] F. Lecocq et al., "Nonreciprocal microwave signal processing with a field-programmable Josephson amplifier," *Phys. Rev. Appl.*, vol. 7, p. 024028, Feb. 2017.
- [48] N. Reiskarimian and H. Krishnaswamy, "Magnetic-free non-reciprocity based on staggered commutation," *Nature Commun.*, vol. 7, no. 4, p. 11217, Apr. 2016.
- [49] J. Zhou, N. Reiskarimian, and H. Krishnaswamy, "Receiver with integrated magnetic-free N-path-filter-based non-reciprocal circulator and baseband self-interference cancellation for full-duplex wireless," in *Proc. IEEE Int. Solid-State Circuits Conf. (ISSCC) Dig. Tech. Papers*, 2016, pp. 178–180.
- [50] N. Reiskarimian, J. Zhou, and H. Krishnaswamy, "A CMOS passive LPTV nonmagnetic circulator and its application in a full-duplex receiver," *IEEE J. Solid-State Circuits*, vol. 52, no. 5, pp. 1358–1372, 2017.
- [51] N. Reiskarimian, M. B. Dastjerdi, J. Zhou, and H. Krishnaswamy, "Highly-linear integrated magnetic-free circulator-receiver

- for full-duplex wireless, in *Proc. IEEE Int. Solid-State Circuits Conf. (ISSCC) Dig. Tech. Papers*, 2017, pp. 316–317.
- [52] N. Reiskarimian, M. B. Dastjerdi, J. Zhou, and H. Krishnaswamy, “Analysis and design of commutation-based circulator-receivers for integrated full-duplex wireless,” *IEEE J. Solid-State Circuits*, vol. 53, no. 8, pp. 2190–2201, 2018.
- [53] T. Dinc, M. Tymchenko, A. Nagulu, D. Sounas, A. Alù, and H. Krishnaswamy, “Synchronized conductivity modulation to realize broadband lossless magnetic-free non-reciprocity,” *Nature Commun.*, vol. 8, no. 10, p. 795, 2017.
- [54] T. Dinc and H. Krishnaswamy, “A 28-GHz magnetic-free non-reciprocal passive CMOS circulator based on spatio-temporal conductance modulation,” in *Proc. IEEE Int. Solid-State Circuits Conference (ISSCC) Dig. Tech. Papers*, 2017, pp. 294–295.
- [55] T. Dinc, A. Nagulu, and H. Krishnaswamy, “A millimeter-wave non-magnetic passive SOI CMOS circulator based on spatio-temporal conductivity modulation,” *IEEE J. Solid-State Circuits*, vol. 52, no. 4, pp. 3276–3292, 2017.
- [56] A. Nagulu, A. Alù, and H. Krishnaswamy, “Fully-integrated non-magnetic 180-nm SOI circulator with >1W P1dB, > +50 dBm IIP3 and high isolation across 1.85 VSWR,” in *Proc. IEEE Radio Frequency Integrated Circuits Symp. (RFIC)*, 2018, pp. 104–107.
- [57] A. Nagulu, T. Dinc, Z. Xiao, M. Tymchenko, D. L. Sounas, A. Alù, and H. Krishnaswamy, “Nonreciprocal components based on switched transmission lines,” *IEEE Trans. Microw. Theory Techn.*, vol. 66, no. 11, pp. 4706–4725, 2018.
- [58] N. Reiskarimian, A. Nagulu, T. Dinc, and H. Krishnaswamy, “Integrated conductivity-modulation-based RF magnetic-free non-reciprocal components: Recent results and benchmarking,” *IEEE Antennas Wireless Propag. Lett.*, vol. 17, no. 11, pp. 1978–1982, 2018.
- [59] N. Chamanara, S. Taravati, Z.-L. Deck-Léger, and C. Caloz, “Optical isolation based on space-time engineered asymmetric photonic band gaps,” *Phys. Rev. B, Condens. Matter*, vol. 96, no. 15, p. 155409, 2017.
- [60] N. A. Estep, D. L. Sounas, and A. Alù, “Magnetless microwave circulators based on spatiotemporally modulated rings of coupled resonators,” *IEEE Trans. Microw. Theory Techn.*, vol. 64, no. 2, pp. 502–518, 2016.
- [61] A. Kord, D. L. Sounas, Z. Xiao, and A. Alù, “Broadband cyclic-symmetric magnet-less circulators and theoretical bounds on their bandwidth. 2018. [Online]. Available: arXiv:1805.01945
- [62] H. Busignies and M. Dishal, “Some relations between speed of indication, bandwidth, and signal-to-random-noise ratio in radio navigation and direction finding,” in *Proc. IRE*, vol. 37, no. 5, pp. 478–488, 1949.
- [63] W. R. Lepage, C. R. Cahn, and J. S. Brown, “Analysis of a comb filter using synchronously commutated capacitors,” *Trans. AIEE, Part I: Commun. Electron.*, vol. 72, no. 1, pp. 63–68, 1953.
- [64] Y. Sun and I. Frisch, “A general theory of commutated networks,” *IEEE Trans. Circuit Theory*, vol. 16, no. 4, pp. 502–508, 1969.
- [65] L. Franks and F. Witt, “Solid-state sampled-data bandpass filters,” in *Proc. IEEE Int. Solid-State Circuits Conf. Dig. Tech. Papers*, 1960, pp. 70–71.
- [66] A. Ghaffari, E. A. M. Klumperink, M. C. M. Soer, and B. Nauta, “Tunable high-Q N-path band-pass filters: Modeling and verification,” *IEEE J. Solid-State Circuits*, vol. 46, no. 5, pp. 998–1010, 2011.
- [67] C. Andrews and A. Molnar, “A passive mixer-first receiver with digitally controlled and widely tunable RF interface,” *IEEE J. of Solid-State Circuits*, vol. 45, no. 12, pp. 2696–2708, 2010.
- [68] N. Reiskarimian, J. Zhou, T. H. Chuang, and H. Krishnaswamy, “Analysis and design of two-port N-path bandpass filters with embedded phase shifting,” *IEEE Trans. Circuits Syst. II, Exp. Briefs*, vol. 63, no. 8, pp. 728–732, 2016.
- [69] M. M. Biedka, R. Zhu, Q. M. Xu, and Y. E. Wang, “Ultra-wide band non-reciprocity through sequentially-switched delay lines,” *Scientific Rep.*, vol. 7, 2017, Art. no. 40014.
- [70] M. M. Biedka, R. Zhu, Q. M. Xu, and Y. E. Wang, “Ultra-wide band on-chip circulators for full-duplex communications,” in *Proc. IEEE/MTT-S Int. Microwave Symp.*, 2018, pp. 987–990.
- [71] J. Krol and S. Gong, “A non-magnetic gyrator utilizing switched delay lines,” in *Proc. IEEE European Microwave Conf.*, 2017, pp. 452–455.
- [72] A. Nagulu and H. Krishnaswamy, “Non-magnetic 60-GHz SOI CMOS circulator-based on loss/dispersion-engineered switched bandpass filters,” in *Proc. IEEE Int. Solid-State Circuits Conf. (ISSCC) Dig. Tech. Papers*, to be published.
- [73] C. Yang and P. Gui, “85–110-GHz CMOS magnetic-free nonreciprocal components for full-duplex transceivers,” *IEEE J. Solid-State Circuits*, pp. 1–12, 2018. [Online]. Available: <https://ieeexplore.ieee.org/document/8519791>
- [74] C. W. Peterson, S. Kim, J. T. Bernhard, and G. Bahl, “Synthetic phonons enable nonreciprocal coupling to arbitrary resonator networks,” *Sci. Advances*, vol. 4, no. 6, p. eaat0232, 2018.
- [75] R. Lu, J. Krol, L. Gao, and S. Gong, “Frequency independent framework for synthesis of programmable non-reciprocal networks,” *Scientific Rep.*, vol. 8, 2018, Art. no. 14655.
- [76] J. Bahamonde, I. Kymissis, A. Alù, and H. Krishnaswamy, “1.95-GHz circulator based on a time-modulated electro-acoustic gyrator,” in *Proc. IEEE Int. Symp. Antennas and Propagation and USNC-URSI Radio Science Meeting*, 2018.
- [77] M. M. Torunbalci, T. J. Odelberg, S. Sridaran, R. C. Ruby, and S. A. Bhawe, “An FBAR circulator,” *IEEE Microw. Compon. Lett.*, vol. 28, no. 5, pp. 395–397, 2018.
- [78] Y. Yu et al., “2.5-GHz highly-linear magnetic-free microelectromechanical resonant circulator,” in *Proc. IEEE Int. Frequency Control Symp. (IFCS)*, 2018.
- [79] G. Mitchetti et al., “A quasi-LTI frequency-selective SAW circulator,” in *Proc. IEEE Int. Ultrasonic Symp. (IUS)*, Oct. 2018, pp. 206–212.
- [80] Y. Yu et al., “Magnetic-free radio frequency circulator based on spatiotemporal commutation of MEMS resonators,” in *Proc. IEEE Micro Electro Mechanical Systems (MEMS)*, 2018, pp. 154–157.
- [81] N. Reiskarimian et al., “A one-way ramp to a two-way highway: Integrated magnetic-free non-reciprocal antenna interfaces for full duplex wireless,” *IEEE Microw. Mag.*, vol. 20, no. 2, pp. 56–75, Feb. 2019.
- [82] J. Zhou et al., “Integrated full duplex radios,” *IEEE Commun. Mag.*, vol. 55, no. 4, pp. 142–151, 2017.
- [83] D. Bharadia, E. McMillin, and S. Katti, “Full duplex radios,” *ACM SIGCOMM Comput. Commun. Rev.*, vol. 43, no. 4, pp. 375–386, 2013.
- [84] A. Sabharwal, P. Schniter, D. Guo, D. Bliss, S. Rangarajan, and R. Wichman, “In-band full-duplex wireless: Challenges and opportunities,” *IEEE J. Sel. Areas Commun.*, vol. 32, no. 9, pp. 1637–1652, 2014.
- [85] A. Shojaefard, K.-K. Wong, M. Di Renzo, G. Zheng, K. A. Hamdi, and J. Tang, “Massive MIMO-enabled full-duplex cellular networks,” *IEEE Trans. Commun.*, vol. 65, no. 11, pp. 4734–4750, 2017.
- [86] M. B. Dastjerdi, S. Jain, N. Reiskarimian, A. Natarajan, and H. Krishnaswamy, “Full-duplex 2x2 MIMO circulator-receiver with high TX power handling exploiting MIMO RF and shared-delay baseband self-interference cancellation,” in *Proc. IEEE Int. Solid-State Circuits Conf. (ISSCC) Dig. Tech. Papers*, 2019, to be published.
- [87] M. B. Dastjerdi, N. Reiskarimian, T. Chen, G. Zussman, and H. Krishnaswamy, “Full duplex circulator-receiver phased array employing self-interference cancellation via beamforming,” in *Proc. IEEE Radio Frequency Integrated Circuits Symp. (RFIC)*, 2018, pp. 108–111.
- [88] B. Park, O. Boric-Lubecke, and V. M. Lubecke, “Arctangent demodulation with DC offset compensation in quadrature Doppler radar receiver systems,” *IEEE Trans. Microw. Theory Techn.*, vol. 55, no. 5, pp. 1073–1079, 2007.
- [89] K.-M. Chen, Y. Huang, J. Zhang, and A. Norman, “Microwave life-detection systems for searching human subjects under earthquake rubble or behind barrier,” *IEEE Trans. Biomed. Eng.*, vol. 47, no. 1, pp. 105–114, 2000.
- [90] J. Marimuthu, K. S. Bialkowski, and A. M. Abbosh, “Software-defined radar for medical imaging,” *IEEE Trans. Microw. Theory Techn.*, vol. 64, no. 2, pp. 643–652, 2016.
- [91] J. Yin et al., “Integrated intravascular optical coherence tomography ultrasound imaging system,” *J. Biomed. Optics*, vol. 15, no. 1, p. 010512, 2010.

